Available online at www.sciencedirect.com
ScienceDirect
Journal of Solid State Chemistry 180 (2007) 1623–1635
JOURNAL OF SOLID STATE CHEMISTRY
www.elsevier.com/locate/jssc

Magnetic structures of the M_2TbF_6 (M = Li, K, Rb) fluorides: A complex behavior resulting from frustration

M. Josse[a,1], M. El-Ghozzi[a,*], D. Avignant[a], G. André[b], F. Bourée[b]

[a]*Laboratoire des Matériaux Inorganiques, UMR 6002 CNRS, Université Blaise Pascal, 63177 Aubière, France*
[b]*Laboratoire Léon Brillouin, CEA-CNRS, CEA-Saclay, 91191 Gif-sur-Yvette, France*

Received 4 September 2006; received in revised form 6 February 2007; accepted 18 February 2007
Available online 28 February 2007

Abstract

Neutron powder diffraction has been performed on Li_2TbF_6, K_2TbF_6 and Rb_2TbF_6 fluoroterbates. Incommensurate long-range magnetic order is observed below $T_N = 2.02$, 1.60 and 2.07 K. The square-modulating of the magnetic structures can be correlated with the geometric frustration induced by the pseudo-hexagonal packing of the $[TbF_6]^{2-}$ chains in these hexafluorides. This frustration and the magnetic interactions are discussed on the basis of experimental data and topological considerations. The magnetic structures encountered in this series, and the particular thermal evolution of the Li_2TbF_6 magnetic structure may result from the competition between the magnetic interactions taking place in the chains and the magnetic interactions coupling the chains.

Keywords: Fluoroterbate; Neutron scattering; Magnetic interactions

1. Introduction

The crystal structure of Li_2TbF_6 was previously established from neutron powder diffraction [1], in order to clarify the unexpected crystal-chemical behavior of this representative within the Li_2MF_6 fluorides divided into four structural families (M = Ge, Ti, Zr and Tb) ([2] and references therein). This compound has been the starting point of an extended study upon the crystal-chemical behavior of the Tb^{4+} ion in fluorides that emphasized the correlation between its electronic configuration and its crystal chemistry [3]. In a preliminary study upon the magnetic properties of the Tb^{4+} ion in Li_2TbF_6, high magnetic field measurements unambiguously confirmed the tetravalent oxidation state of the terbium in this compound [4], (Tb^{4+}: $4f^7$ electronic configuration and $^8S_{7/2}$ ground state). In a previous early report [5], a few statements about the magnetic structures of K_2TbF_6 and Rb_2TbF_6 were established. This work deals with the crystal structures of K_2TbF_6 and Rb_2TbF_6 and the magnetic structure of the M_2TbF_6 (M = Li, K, Rb) fluorides investigated by neutron powder diffraction. The outstanding structural feature of these compounds is the presence of infinite $[TbF_6]^{2-}$ chains built of edge-sharing $[TbF_8]^{4-}$ polyhedra and arranged in a pseudo-hexagonal packing. This induces a pronounced one-dimensional character that offers the opportunity to investigate the nature of the magnetic interactions occurring in these compounds. Furthermore, the pseudo-hexagonal packing of the $[TbF_6]^{2-}$ chains should lead to geometric frustration of the interchain magnetic interactions. Through this study, magnetic behavior in these M_2TbF_6 (M = Li, K, Rb) compounds will be discussed, with a particular focus on Li_2TbF_6 as well as correlations between nuclear and magnetic structures from topological analysis.

2. Experimental

Polycrystalline samples were obtained by heating overnight stoichiometric mixtures of MF (Strem chemicals) and TbF_4 (prepared by fluorination of Tb_4O_7, (Merck)), under pure fluorine gas, at 500 °C. The samples were then annealed for 12 h at 550 °C to ensure a uniform homogeneity.

*Corresponding author. Fax: +33 4 73 40 71 08.
E-mail address: Malika.EL-GHOZZI@univ-bpclermont.fr (M. El-Ghozzi).
[1]Present address: Institut de Chimie de la Matière Condensée de Bordeaux, UPR 9048 CNRS, 33608 Pessac, France.

0022-4596/$ - see front matter © 2007 Elsevier Inc. All rights reserved.
doi:10.1016/j.jssc.2007.02.011

Neutron powder diffraction patterns were recorded at the Orphee reactor (Laboratoire Léon Brillouin, Saclay, France) on the two-axis G4.1 diffractometer ($\lambda = 2.426$ Å) in the range $15 \leqslant 2\theta \leqslant 95^\circ$ (time scan: 2 h, step scan: 0.1°), with increasing temperature in the range 1.4–5.0 K, without any magnetic field, for the determination of the magnetic structures [6] and at 300 K on the high-resolution 3T2 diffractometer ($\lambda = 1.225$ Å) in the range $6 \leqslant 2\theta \leqslant 126^\circ$ (time scan: 24 h, step scan: 0.05°) [6] for the refinement of K_2TbF_6 and Rb_2TbF_6 crystal structures. Rietveld refinements were performed with the FULLPROF program [7], and for the magnetic contributions, magnetic form factors of the Tb^{3+} ion were used for the Tb^{4+} one as previously justified [8].

3. Results and discussion

3.1. Nuclear structures

3.1.1. Refinement at room and low temperatures

The crystal structures of K_2TbF_6 [9] and Rb_2TbF_6 [10] have previously been investigated by powder XRD, and were found to be isostructural with K_2ZrF_6 [11], whereas Li_2TbF_6, as shown by a neutron powder diffraction study [1], crystallizes with the β high-pressure form of Li_2ZrF_6 [12]. The Rietveld refinements of K_2TbF_6 and Rb_2TbF_6 neutron data at $T = 300$ K confirmed the models previously established (Fig. 1a and b) with $R_{Bragg} = 4.61\%$ and 4.10%, respectively (Table 1).

Neutron powder diffraction patterns of the title compounds have also been recorded at low temperature on the G4-1 diffractometer in the paramagnetic state. No structural phase transition was observed during the cooling. The nuclear structures have successfully been refined at

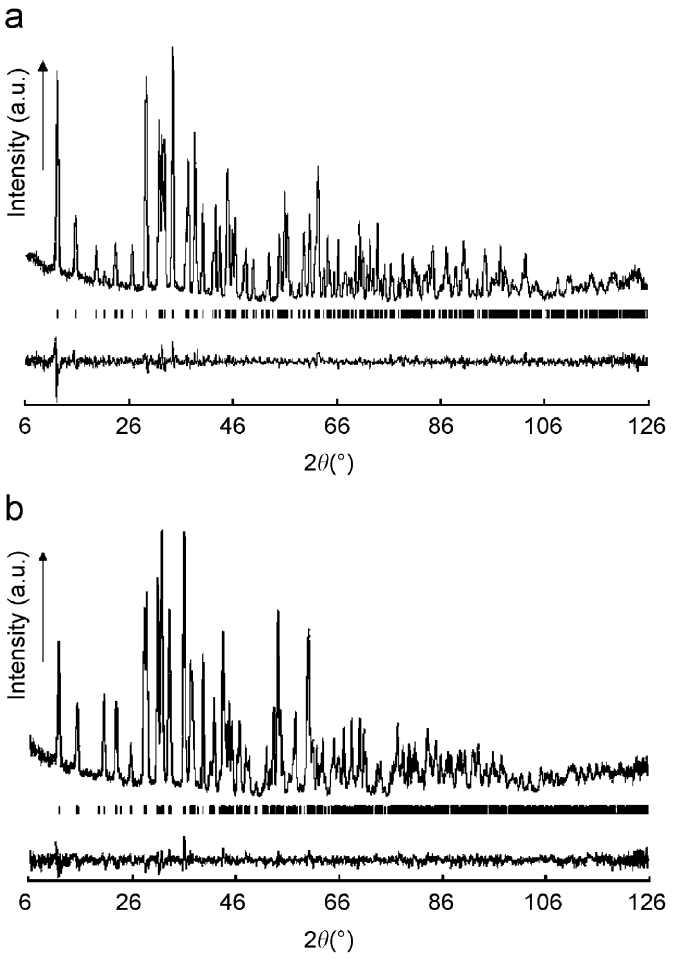

Fig. 1. Rietveld plot (2θ, deg) of the crystal structure refinement (300 K) for K_2TbF_6 (a) and Rb_2TbF_6: observed (dotted line), calculated (solid line) and difference patterns (Bragg positions are indicated by the vertical bars) ($\lambda = 1.2251$ Å).

Table 1
Details of the Rietveld refinements (nuclear structures) of K_2TbF_6 and Rb_2TbF_6 at 300 K

Compound	K_2TbF_6	Rb_2TbF_6
Symmetry	Monoclinic	
Space group	$C2/c$ (no. 15)	
Z	4	
Cell parameters (Å)	$a = 6.6182(1)$	$a = 6.8557(1)$
	$b = 11.4898(2)$	$b = 11.9207(2)$
	$c = 7.1435(1)$	$c = 7.2237(1)$
	$\beta = 90.239(1)$	$\beta = 91.123(1)$
Cell volume (Å^3)	543.20(1)	590.24(2)
Wavelength	1.2251 Å	
Angular range/step (2θ)	6.00–125.70°/0.05	
Independent reflections	893	977
Intensity-dependent parameters	18	18
Conventional reliability factors (%)		
R_F	3.43	3.09
R_B	4.61	4.10
R_P	11.2	10.2
R_{wp}	10.2	9.54

Table 2
Characteristics of the Rietveld refinement (nuclear structure) of the M_2TbF_6 fluorides at low temperature

Compound (T)	Li_2TbF_6 (4 K)	K_2TbF_6 (5 K)	Rb_2TbF_6 (5 K)
Symmetry	Monoclinic	Monoclinic	Monoclinic
Space group	$P2_1/c$ (no 14)	$C2/c$ (no 15)	$C2/c$ (no 15)
Z	4	4	4
Refined cell parameters	$a = 7.5630(2)$ Å	$a = 6.5909(2)$	$a = 6.8299(2)$
	$b = 4.9361(2)$ Å	$b = 11.4135(4)$	$b = 11.8385(5)$
	$c = 11.0704(5)$ Å	$c = 7.1235(2)$	$c = 7.2013(2)$
	$\beta = 107.007(3)^\circ$	$\beta = 90.502(2)$	$\beta = 91.358(2)$
Cell volume (Å^3)	395.21(3)	535.84(3)	590.24(2)
Wavelength	2.4266 Å		
2θ range/step	15–95°/0.1		
Independent reflections	90	83	62
Intensity-dependent parameters	28	13	16
Conventional reliability factors (%)			
R_F	1.98	1.23	1.69
R_B	2.01	1.81	2.44
R_p	11.5	9.55	9.09
R_{wp}	11.3	9.45	9.38

Table 3
Atomic coordinates for the M_2TbF_6 ((a): M = K, Rb, (b): M = Li) fluorides, obtained from X-rays and neutron powder diffraction data (italic), at room and low temperature

(a)

Compound		K_2TbF_6			Rb_2TbF_6		
Atoms and sites		x	y	z	x	y	z
M	(RX)	0.006(2)	0.331(2)	−0.008(2)	0.0213(7)	0.3426(5)	0.0053(7)
8*f*	(*N*)	0.0211(6)	0.3397(3)	0.0039(6)	0.0214(3)	0.3422(2)	0.0021(3)
	(*N*, 5*K*)	0.025(2)	0.340(1)	0.999(2)	0.026(1)	0.3429(5)	0.0007(8)
Tb	(RX)	0	0.0445(3)	1/4	0	0.0440(3)	1/4
4*e*	(*N*)	0	0.0452(2)	1/4	0	0.0447(2)	1/4
	(*N*, 5*K*)	0	0.0470(4)	1/4	0	0.0445(5)	1/4
F1	(RX)	0.327(2)	−0.024(2)	0.212(3)	0.290(3)	−0.010(2)	0.229(3)
8*f*	(*N*)	0.2942(4)	0.9824(2)	0.2071(4)	0.2861(4)	0.9840(2)	0.2221(4)
	(*N*, 5*K*)	0.2931(9)	0.9813(6)	0.207(1)	0.287(1)	0.9838(6)	0.2162(9)
F2	(RX)	0.176(1)	0.202(1)	0.261(4)	0.191(3)	0.187(2)	0.298(3)
8*f*	(*N*)	0.1942(4)	0.1921(2)	0.2779(3)	0.1870(4)	0.1872(2)	0.2780(4)
	(*N*, 5*K*)	0.192(1)	0.1934(6)	0.282(1)	0.187(1)	0.187(6)	0.282(1)
F3	(RX)	−0.016(2)	0.1059(9)	0.544(2)	−0.050(3)	0.094(1)	0.541(3)
8*f*	(*N*)	0.9559(4)	0.1008(2)	0.5446(9)	0.9644(4)	0.0964(2)	0.5428(3)
	(*N*, 5*K*)	0.951(1)	0.1011(8)	0.5463(7)	0.962(1)	0.0970(6)	0.5417(8)

(b)

Atoms and sites		Li_2TbF_6		
		x	y	z
Li1	(*N*)	0.405(2)	0.501(8)	0.326(2)
4*e*	(*N*, 4*K*)	0.402(7)	0.49(1)	0.305(5)
Li1	(*N*)	0.036(3)	−0.033(8)	0.194(2)
4*e*	(*N*, 4*K*)	0.029(8)	−0.04(1)	0.152(5)
Tb	(*N*)	0.2534(3)	0.5135(2)	0.0016(2)
4*e*	(*N*, 4*K*)	0.252(3)	0.512(2)	−0.000(1)
F1	(*N*)	0.459(1)	0.185(2)	0.4275(9)
4*e*	(*N*, 4*K*)	0.456(2)	0.196(4)	0.422(2)
F2	(*N*)	0.102(1)	0.357(1)	0.8215(8)
4*e*	(*N*, 4*K*)	0.105(4)	0.367(3)	0.827(2)
F3	(*N*)	0.047(1)	0.238(2)	0.5431(8)
4*e*	(*N*, 4*K*)	0.044(3)	0.223(6)	0.541(1)
F4	(*N*)	0.408(2)	0.223(2)	0.6570(9)
4*e*	(*N*, 4*K*)	0.405(4)	0.234(4)	0.657(2)
F5	(*N*)	0.248(1)	0.631(1)	0.3969(7)
4*e*	(*N*, 4*K*)	0.249(2)	0.629(4)	0.402(2)
F6	(*N*)	0.248(1)	0.755(1)	0.6597(9)
4*e*	(*N*, 4*K*)	0.251(2)	0.750(4)	0.656(2)

low temperature, using the structural models determined at room temperature: $R_{Bragg} = 2.0\%$, 1.8% and 2.4% for Li_2TbF_6, K_2TbF_6 and Rb_2TbF_6, respectively (Table 2).

The atomic coordinates obtained from neutron powder diffraction data confirm the previously obtained results from XRD and allow a more accurate description of the anionic sublattices (Table 3).

3.1.2. Nuclear structures and topology of the M_2TbF_6 fluorides (M = Li, K, Rb)

In Li_2TbF_6, the Tb^{4+} ions adopt an eight-coordinated environment having a dodecahedral configuration. Each $[TbF_8]^{4-}$ polyhedron shares two opposite edges with two adjacent polyhedra to form infinite $[TbF_6]^{2-}$ pleated chains. These chains are arranged in a

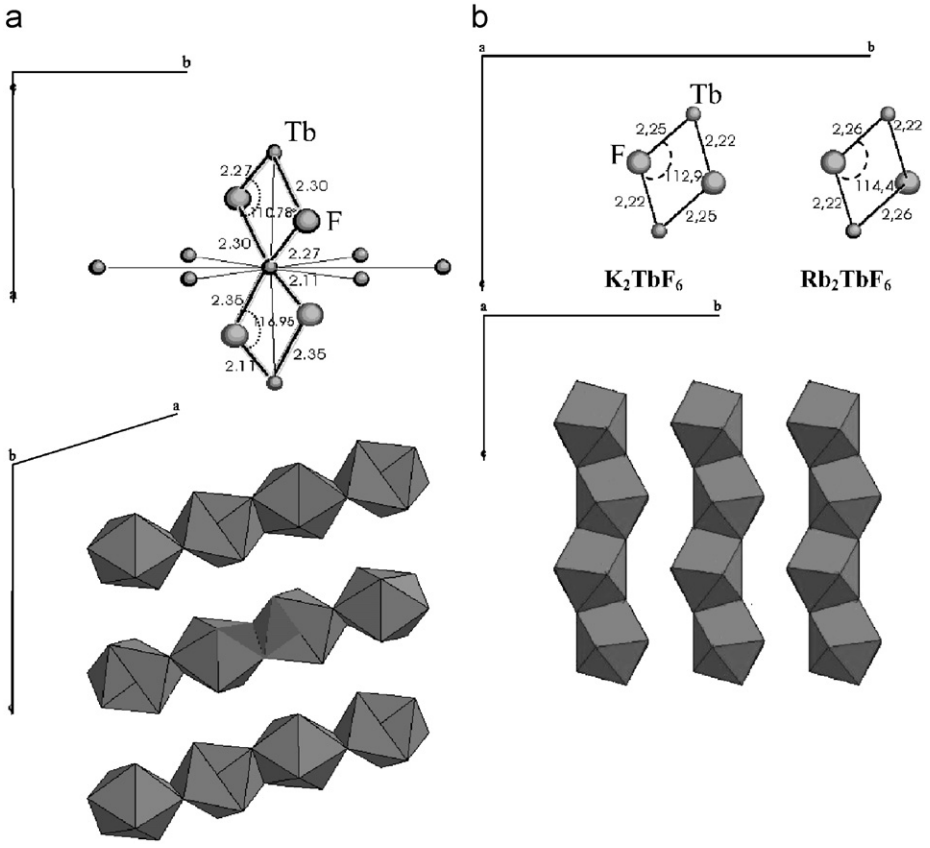

Fig. 2. View of the $[TbF_6]^{2-}$ chains and their topology in the M_2TbF_6 ((a) Li and (b) K, Rb) series.

pseudo-hexagonal packing and further joined by the lithium ions.

The polyhedral linkings in K_2TbF_6 and Rb_2TbF_6 are similar to that of Li_2TbF_6, except the eight fluorine atoms surrounding the Tb^{4+} ions form slightly distorted square antiprisms (see Figs. 2 and 3). Table 4 summarizes the room-temperature topological characteristics of the polyhedral linkings encountered in the M_2TbF_6 fluorides. It is worth noticing that the two Tb ions and the two F ions involved in edge sharing between $[TbF_8]^{4-}$ polyhedra (Fig. 2) are coplanar in the three compounds.

From the magnetic point of view, two outstanding features evolve from these M_2TbF_6 fluorides series:

- their one-dimensional character,
- the pseudo-hexagonal packing of the infinite $[TbF_6]^{2-}$ chains leading to significant frustration of the magnetic interchain interactions.

Moreover, the geometric frustration may be expected to be weaker for Li_2TbF_6 due to the more irregular pseudo-hexagonal packing of the chains.

3.2. Magnetic structures

3.2.1. Magnetic structure of Li_2TbF_6 at 1.43 K

3.2.1.1. Resolution. From neutron diagrams recorded at temperatures between 1.43 and 2 K, a long-range antiferromagnetic order has been evidenced from a large number of sharp pure magnetic peaks. The particular position of several of them, on both sides of some nuclear Bragg reflections, suggests that these peaks are satellite peaks arising from an incommensurate magnetic structure, and the quasi-superposition of few of them with nuclear peaks reflects a long period (Fig. 4). All the magnetic peaks could have been indexed using a single component propagation vector $\vec{k} = (0k_y0)$, and this component was refined to $k_y = 0.01626(6)$ at 1.43 K. It should be noticed that the propagation vector is collinear to the direction along which the interchain distances are the shortest (4.93 Å).

The quasi-superposition (with nuclear peaks) of magnetic Bragg positions generated by this propagation vector, associated with the low monoclinic symmetry, did not allow a simple determination of the magnetic moment direction by analyzing systematic absence in the magnetic diffraction pattern. As the terbium ions occupy the general Wyckoff position of the $P2_1/c$ space group, their magnetic moments are free of any symmetry constraint. The main component of the magnetic moment of the Tb^{4+} ions was found to be parallel to the *a*-axis, along which the $[TbF_6]^{2-}$ chains extend. Considering the orientation of the propagation vector ($k_y = 0.01626(6)$, corresponding to the shortest interchain distance), and the fact that modulated magnetic structures are frequently observed in hexagonal arrays [13], a modulation propagating from chain to chain has been

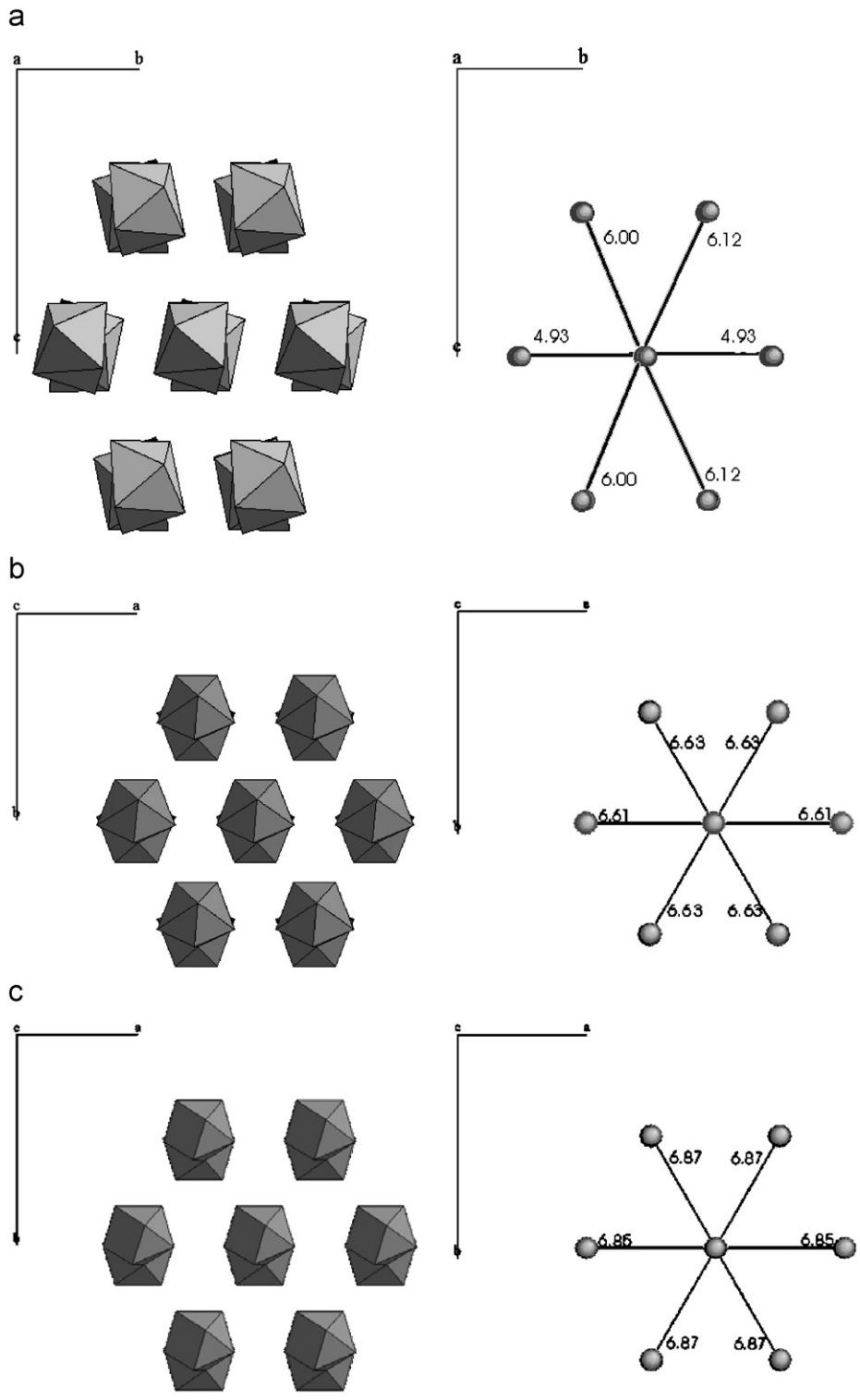

Fig. 3. Pseudo-hexagonal packing of the $[TbF_6]^{2-}$ chains in the M_2TbF_6 series ((a) Li, (b) K, (c) Rb).

envisaged. This modulation was chosen sinusoidal, as the calculated intensities associated with a helicoidal magnetic structure were inconsistent with the observed pattern. A Rietveld refinement of this hypothesis gave consistent but yet unsatisfactory result, as several magnetic peaks were badly fit or even not taken into account. The introduction of a small magnetic contribution along the *b*-axis did not fit with the experimental data. Better results were obtained with an additional component along the *c*-axis, the resulting moment of the Tb^{4+} ions being in the *a*–*c* plane.

However, a careful examination of the experimental data found an unusual broadness of the base of several magnetic

peaks (Fig. 4), namely those indexed $h\,k\,l$ with $k \neq 0$, contrary to the $h\,0\,l$ reflections. This selective "shouldering" can be correlated to the propagation vector $\vec{k} = (0, 0.01626(6), 0)$ and suggests the existence of high-order magnetic satellites (third and even fifth), which are not significantly separated from first-order magnetic satellites and nuclear Bragg peaks when these belong to the $h\,0\,l$ family. By introducing the third harmonic the refinement was sensibly improved, but some significant contributions were still not taken into account and the introduction of the fifth-order harmonic of the sinusoidal modulation in the refinement led to $R_{mag} = 3.86\%$ and $R_{nuc} = 4.05\%$ at 1.43 K (Fig. 5), with a propagation vector $\vec{k} = (0\ 0.01620(7)\ 0)$ and an overall magnetic moment of $6.4(1)\,\mu_B$ for Tb^{4+} ions.

Table 4
Topological details concerning crystal structures of the M_2TbF_6 fluorides

Compound	Distances (Å)		Angles (deg)		
	Interchain Tb–Tb	Intrachain Tb–Tb	Edges environment		Intrachain consecutive edges (dihedral)
			Tb–F	Tb–F–Tb	
Li_2TbF_6	4.93	3.76	2.27	110.8	
$T_N = 2.02$ K	6.00		2.30		61.6
	6.12	3.81	2.11	117.0	
			2.35		
K_2TbF_6	6.61		2.22		
$T_N = 1.60$ K	6.63 ($\times_2$)	3.71 ($\times_2$)	2.25	112.9	41.0
Rb_2TbF_6	6.85		2.22		
$T_N = 2.07$ K	6.87 ($\times_2$)	3.76 ($\times_2$)	2.26	114.4	38.2

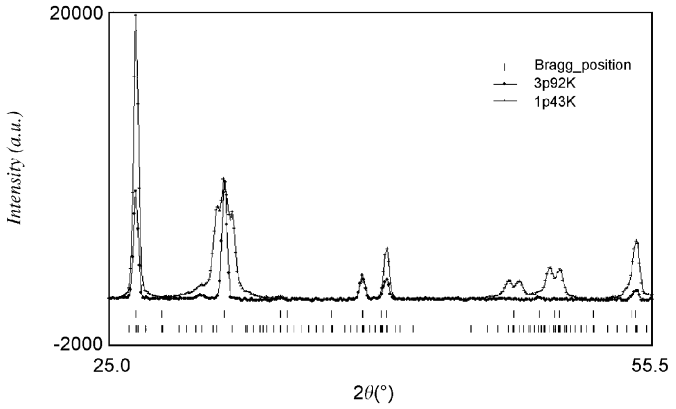

Fig. 4. Part of the neutron diffraction patterns (NDP) of Li_2TbF_6 at 3.92 K (·) and 1.43 K (+), vertical bars: Bragg positions, nuclear (upper) and magnetic (lower) ($\lambda = 2.4266$ Å).

The summation of the first-, third- and fifth-order sinusoidal harmonics (the amplitudes of which, with respect to the first harmonic, are in the ratio 1/1, 1/3 and 1/5, respectively) generates an incommensurate square-modulated magnetic structure expanding through more than 61 nuclear cells (Fig. 6).

3.2.1.2. Thermal evolution of Li_2TbF_6 magnetic structure. The thermal evolution of modulated magnetic structures may be characterized by a change in their period (i.e. lock-in transition from incommensurate to commensurate), or/and by a change in their nature (i.e. transition from a sine- to a square-modulated magnetic structure) [13]. Four additional neutron diagrams recorded at 1.48, 1.70, 1.84 and 1.94 K were used to study the thermal evolution of the Li_2TbF_6 magnetic structure. If the thermal evolution of the observed intensities of the $0\,0\,2^{\pm}$ satellites is in agreement with $T_N = 2.02(1)$ K (Fig. 7), the thermal evolution of the propagation vector $\vec{k} = (0k_y0)$ exhibits a significant singularity at $T = 1.43$ K (Fig. 8). From 1.94 K and down to 1.48 K the value of k_y is actually close to 0.0182(1) (i.e. a period of more than 54 nuclear cells), but at 1.43 K the refined value of k_y is 0.01617(7) (i.e. a period of more than 61 nuclear cells). This peculiar behavior is clearly illustrated by Fig. 9 where a sensible displacement

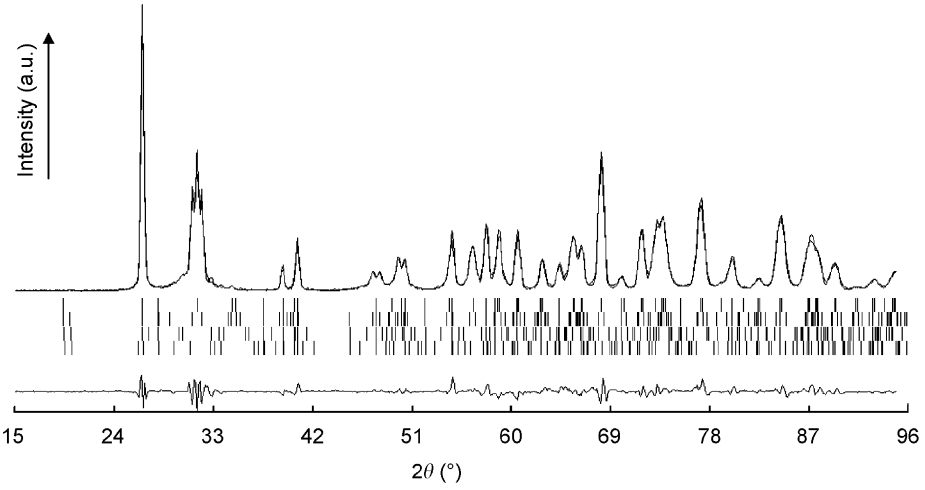

Fig. 5. Rietveld refinement of the magnetic structure of Li_2TbF_6 at 1.43 K: observed (dotted line) calculated (solid line) and difference patterns (magnetic Bragg positions are indicated by the lower vertical bars) ($\lambda = 2.4266$ Å).

Fig. 6. Schematic representation of Li_2TbF_6 magnetic structure (the nuclear cell is represented by the gray rectangle).

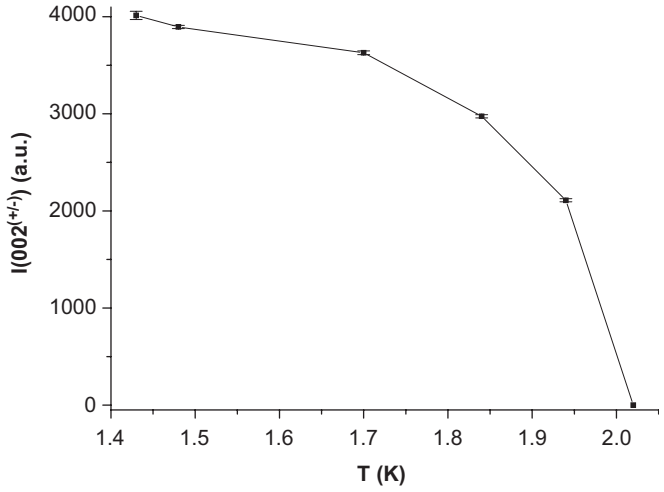

Fig. 7. Thermal variation of the observed intensity of the $002^{\pm}$ magnetic satellite for Li_2TbF_6.

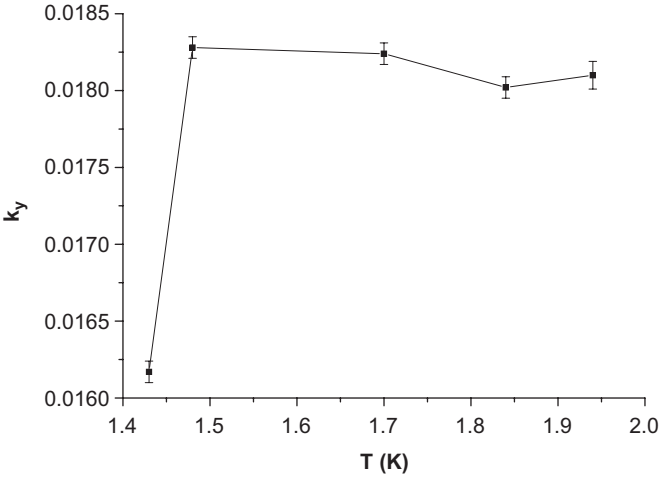

Fig. 8. Thermal variation of the k_y component of the propagation vector for Li_2TbF_6.

of the first-order satellites closer to the nuclear peak is observed at 1.43 K. This displacement, also observed in the preliminary diagrams recorded with decreasing temperatures, is characteristic of a greater period of the incommensurate magnetic structure. Rietveld refinements revealed that the square-modulated magnetic structure seems to persist up to the ordering temperature (i.e. the three odd harmonics persist). According to these refinements, the direction of the resulting magnetic moment seems to remain stable within this temperature range (taking into account the experimental uncertainties). Therefore, the discontinuity observed below 1.48 K is hardly ascribable to a magnetic phase transition.

3.2.2. Magnetic structures of K_2TbF_6 and Rb_2TbF_6 at 1.4 K

3.2.2.1. Refinement. Low-temperature ($1.4\,K \leqslant T < 5\,K$) neutron diffraction powder patterns revealed the existence of a long-range magnetic order below $T \approx 1.6$ and 2.1 K for K_2TbF_6 and Rb_2TbF_6, respectively (Fig. 10). As mentioned in our early report, the magnetic structures of K_2TbF_6 and Rb_2TbF_6 are similar to that of Li_2TbF_6. In this work refinements were performed using the full set of diffraction data (nuclear and magnetic), allowing much more reliable results. The magnetic structure was refined using a wave vector $\vec{k} = (k_x 00)$ collinear to the shortest interchain distances, associated with first-, third- and fifth-order satellites of a sinusoidal modulation, and a magnetic moment collinear to the binary axis (as the Tb^{4+} ions lie on the binary axis [14]). The wave vectors associated with these magnetic structures are $\vec{k} = (0.0074(2)\ 0\ 0)$, i.e., a magnetic structure expanding over more than 130 nuclear cells, and $\vec{k} = (0.01040(8)\ 0\ 0)$ (more than 90 nuclear cells) for K_2TbF_6 and Rb_2TbF_6, respectively.

The reliability factors for the first harmonic (see Table 5 for third and fifth harmonics) converged to the final values: $R_{mag} = 2.43\%$ and $R_{mag} = 2.17\%$, with $\mu_{Tb4+} = 4.44(6)\,\mu_B$ and $\mu_{Tb4+} = 6.27(5)\,\mu_B$ ($\mu_{th.} = 7.0\,\mu_B$) for K_2TbF_6 and Rb_2TbF_6, respectively (Fig. 11 and Table 5). The low ordering temperature of K_2TbF_6 implies that at $T = 1.4$ K the sample was still magnetically unsaturated, accounting for the small value of the observed magnetic moment.

3.2.2.2. Thermal evolution. Several neutron diffraction patterns have been recorded between 1.4 K and the ordering temperatures for K_2TbF_6 and Rb_2TbF_6, in order to investigate the evolution of their magnetic structures. The thermal evolution of the $(110)^+$ satellite-integrated intensity is consistent with $T_N = 1.60(2)$ K for K_2TbF_6 (Fig. 12a) and $T_N = 2.07(2)$ K for Rb_2TbF_6 (Fig. 12b). In K_2TbF_6, the growth of this satellite presents an inverted curvature, in contrast with what is usually observed. Contrary to Li_2TbF_6, the propagation vectors are almost constant (within the experimental uncertainties) with increasing temperature for the two compounds. As for Li_2TbF_6, the Rietveld refinements confirmed that the square-modulated magnetic structures are stable up to the ordering temperature, the magnetic moment direction and the relative amplitudes of the magnetic harmonics remaining stable in this temperature range.

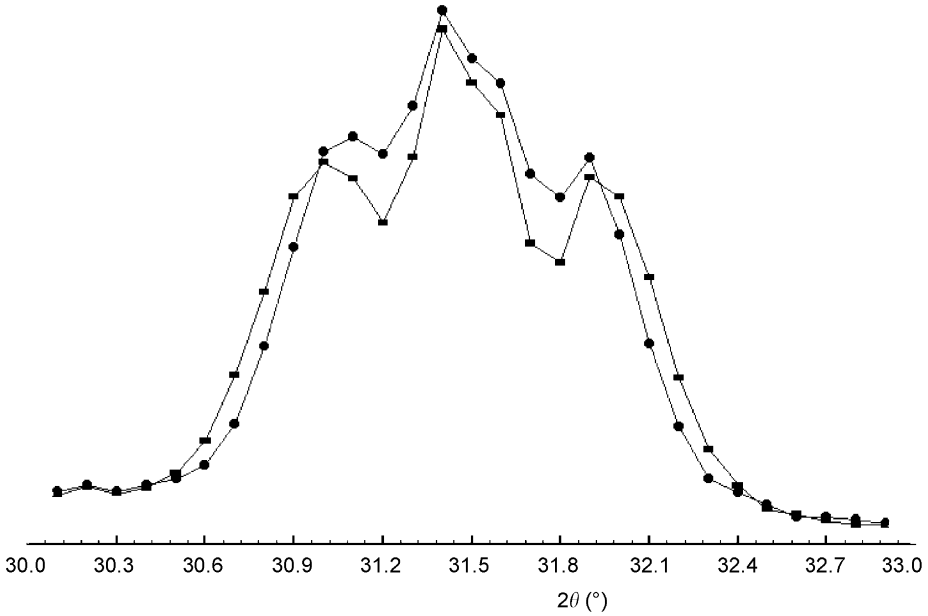

Fig. 9. Part (30–33°, 2θ) of the NDP of Li_2TbF_6 (0 0 2 nuclear peak and magnetic satellites) at 1.48 K (■) and 1.43 K (●) ($\lambda = 2.4266$ Å).

3.3. Discussion

3.3.1. Frustration and magnetic behavior of the M_2TbF_6 fluorides

The incommensurate magnetic structures observed in the M_2TbF_6 series, characterized by long periods (more than 130 nuclear cells in K_2TbF_6), has been related to the pseudo-hexagonal packing of the infinite $[TbF_6]^{2-}$ chains as was suggested in our early report [5]. Because of the frustration induced by this topology, the antiferromagnetic interactions coupling the ferromagnetic $[TbF_6]^{2-}$ chains cannot be compensated to lead to a short period commensurate magnetic structure.

In order to allow a better understanding of the magnetic behavior of the $MTbF_6$ compounds, let us come back on the relationship between the topology and magnetic interactions. The relative values of the ordering temperatures observed in this series suggest a narrow interplay between the geometric frustration and the interchain interactions. The increase of the modulation period may be understood considering the geometric frustration resulting from spin chains arranged in a pseudo-hexagonal packing. As the temperature decreases, the magnetic interactions coupling the $[TbF_6]^{2-}$ chains play a more and more important role, as well as the magnetic frustration arising from the pseudo-hexagonal packing of these chains. Therefore, the equilibrium configuration between the spin chains is harder to reach and may induce a longer period of the incommensurate magnetic structure.

From the above considerations, the nature of the magnetic interactions taking place in the M_2TbF_6 fluorides may be examined. For 1D magnetic materials built of isolated magnetic chains, two exchange integrals are generally taken into account: J_{intra} and J_{inter}. The ratio of these integrals may lead to a theoretical evaluation of the ordering temperature [15], which can reach substantially high values for d elements. In our case the ordering temperatures are very low and no ordering temperature reaches the liquid helium temperature in fluoroterbates up to now [16]. Thus it could be assumed that both J_{intra} and J_{inter} are of the same order of magnitude in the M_2TbF_6 series. As the rare-earth magnetism is generally dominated by dipolar interactions, the predominant interaction, either J_{intra} or J_{inter}, may be questioned. To answer this question let us consider values gathered in Table 4. It can be seen that for similar environments occurring in the M_2TbF_6 series, the shortest Tb–Tb distance within the chain is associated with the lowest ordering temperature (K representative). This confirms that the long-range magnetic ordering does not solely depend on the intrachain interactions but also on the chains coupling interactions. Since the alkali ions are likely not relaying any exchange interactions, contrary to what is currently observed in more covalent substances like phosphates for instance [17], dipolar interactions should be the only couplings between the chains. Thus the interchain interactions should be an important parameter governing the overall magnetic behavior of the M_2TbF_6 compounds.

At this stage it is worth to emphasize that the $[TbF_6]^{2-}$ chains may be considered as the magnetic object from which the magnetic structure is built, for in one $[TbF_6]^{2-}$ chain all the spins adopt the same orientation.

From the aforementioned considerations, as the interchain distances increase from Li to Rb, the ordering temperatures should decrease accordingly, since dipolar interactions are directly dependent on the dipole–dipole distances. This trend is not experimentally observed, in particular for K and Rb representatives, and the evolution

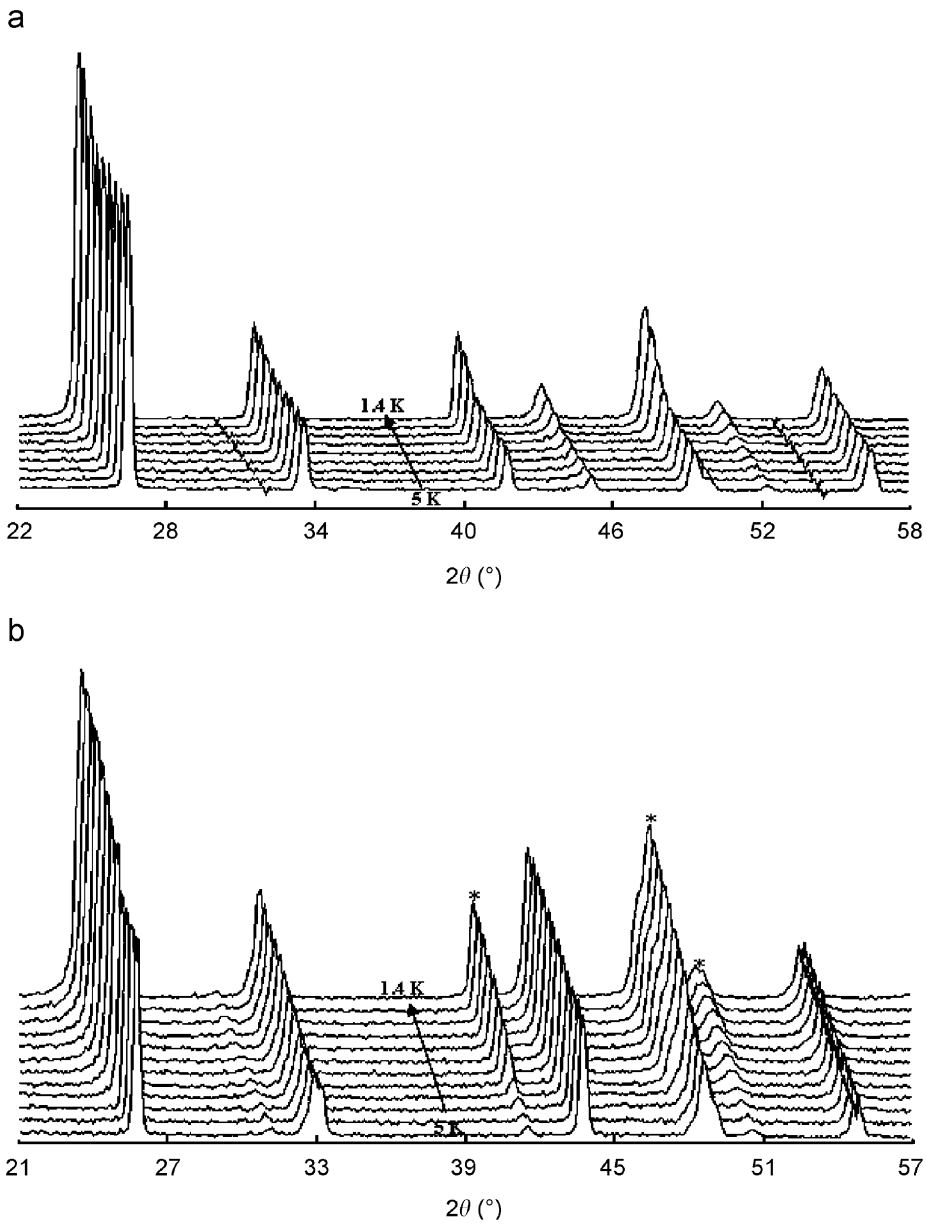

Fig. 10. Thermal evolution of K_2TbF_6 (a) and Rb_2TbF_6 (b) part of the NDP (2θ, deg) *: magnetic satellites revealing the incommensurate structure ($\lambda = 2.4266$ Å).

of the topological frustration in the series should be considered to explain the experimental ordering temperatures. Although this point was briefly treated in our early report [5], it is worth coming back on this interplay. The pseudo-hexagonal packing of the $[TbF_6]^{2-}$ chains in Li_2TbF_6 is irregular enough (Fig. 3), whereas the departure from an ideal hexagonal array for the K and Rb compounds is rather insignificant. Therefore, in Li_2TbF_6 the geometric frustration is weakened by the departure from a regular hexagonal packing of the chains, whereas it is enhanced by the quasi-regular ones in both K_2TbF_6 and Rb_2TbF_6.

Let us remember that Li_2TbF_6 is not isostructural with the two other representatives in the series, and therefore a direct comparison of the ordering temperatures of these compounds could not be assessed in a rigorous way.

Taking into account the strength of the interchain interactions and the efficiency of the frustration, although this point was briefly treated in our early report [5], it is worth coming back on this interplay, the ordering temperature of each representative of the series may be rationalized as follows:

- In Li_2TbF_6, the weakened frustration and the stronger interchain couplings, allow the onset of a long-range magnetic order at 2.02(1) K.
- In K_2TbF_6, the strong frustration is efficiently relayed by interchain interactions and repels the onset of the long-range magnetic order down to 1.60(2) K.

Table 5
Details of the magnetic structures refinements of the M_2TbF_6 fluorides

Compound	Li_2TbF_6	K_2TbF_6	Rb_2TbF_6
Refined cell parameters	$a = 7.5636(3)$ Å $b = 4.9373(2)$ Å $c = 11.0701(3)$ Å $\beta = 107.017(3)^\circ$	$a = 6.5920(3)$ Å $b = 11.4147(5)$ Å $c = 7.1239(3)$ Å $\beta = 90.509(2)^\circ$	$a = 6.8302(2)$ Å $b = 11.8393(4)$ Å $c = 7.2005(2)$ Å $\beta = 91.357(2)^\circ$
Propagation vectors	$k_y = 0.01626(6)$	$k_x = 0.0074(2)$	$k_x = 0.01040(8)$
Wavelength	2.4266 Å		
θ range/step	15–95°/0.1		
Independent reflections	1670	1437	1548
Intensity-dependent parameters	2	1	1
Conventional Rietveld reliability factors (%)			
R_F	2.54	1.06	0.677
R_B	4.05	1.78	1.18
R_{mag} (first harmonic)	3.86	2.43	2.17
Third/fifth harmonics	8.77/11.9	7.26/12.5	5.93/10.8
R_p	10.5	8.73	6.98
R_{wp}	11.6	9.11	7.80

- In Rb_2TbF_6, due to the longer interchain distances, the strong frustration is badly relayed by weaker interchain interactions, so that the ordering temperature (2.07(2) K) is less affected by the frustration.

3.3.2. Magnetic behavior of Li_2TbF_6 and magnetic interactions

Another interesting feature is the unexpected thermal evolution of the Li_2TbF_6 magnetic structure, which may also be understood as a competition, arising from geometric frustration, between the magnetic interactions coupling the Tb^{4+} ions. Indeed, if magnetic dipolar interactions between the chains are strongly predictable, the nature of the Tb^{4+}–Tb^{4+} magnetic interactions within the chains should be examined.

A discontinuity is observed in the thermal evolution of the propagation vector below $T = 1.48$ K (Fig. 8). As the dipolar interaction alone should result in a continuous thermal variation, this behavior sustains the possible existence of exchange interactions in the chains. This hypothesis is supported by the observation of one-dimensional magnetic correlations above T_N. Comparison of neutron diffraction patterns obtained at 2.18 and 3.92 K shows an obvious diffuse scattering signal between $32 \leqslant 2\theta \leqslant 40^\circ$ in the lowest temperature diagram. The observed signal shown in Fig. 13 may arise from the diffusion by a periodic one-dimensional array of a few identical scatterers, i.e., this signal should be characteristic of short-range one-dimensional magnetic correlation in spin chains. This observation agrees with differentiated

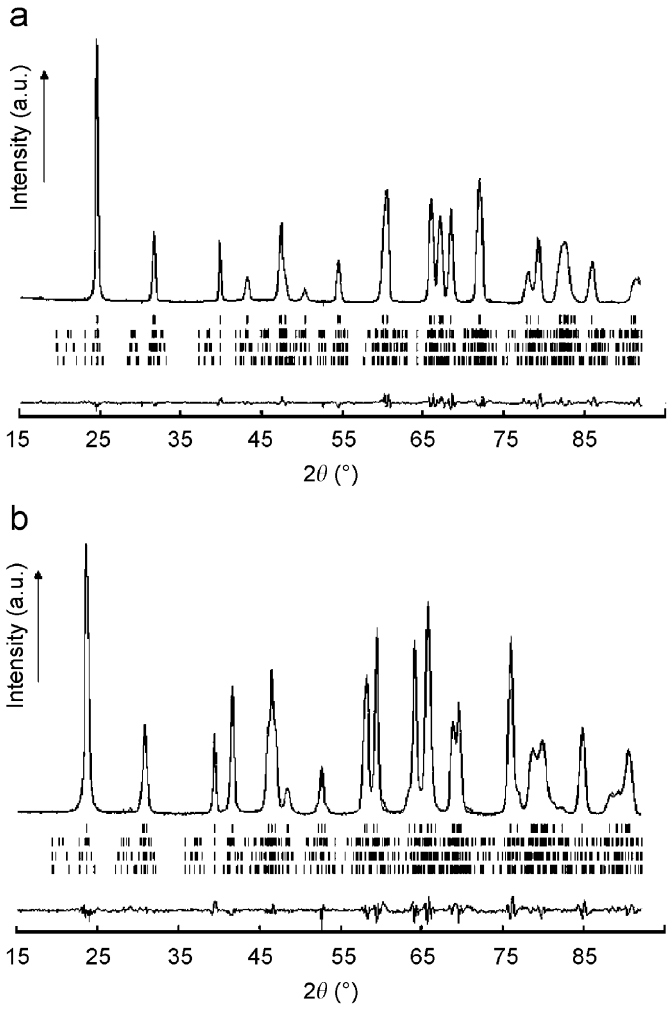

Fig. 11. Rietveld plot (2θ, deg) of the magnetic structure refinement of K_2TbF_6 (a) and Rb_2TbF_6 (b) at 1.4 K: observed (dotted line) calculated (solid line) and difference patterns (magnetic Bragg positions are indicated by the three lowest vertical bars) ($\lambda = 2.4266$ Å).

magnetic interactions in the chains (exchange interactions), and between the chains (dipolar interactions). Moreover, the diffusion signal is centered around $2\theta = 36^\circ$, which corresponds to an interreticular distance of 3.9 Å, in relatively good agreement with the average Tb–Tb distance of 3.79 Å in the chain. Additional considerations reinforce the assumption of superexchange couplings. The internal character of the $4f$ orbitals and their weak spatial expansion excludes the existence of direct $4f$–$4f$ exchange interactions, for Tb–Tb distances about 3.8 Å in the chains. Magnetic anisotropy may no longer be invoked to explain this behavior, as the singlet ground state $^8S_{7/2}$ of the Tb^{4+} ion is not affected by such interaction. Intrachains interactions are probably relayed by the fluoride ions which delimit the shared edges between the $[TbF_8]^{4-}$ polyhedra. In a larger field of investigation, phenomenological considerations allowed us to state an empirical rule correlating the magnetic behavior of terbium fluorides to their Polyhedra Connection Mode (PCM) [18]:

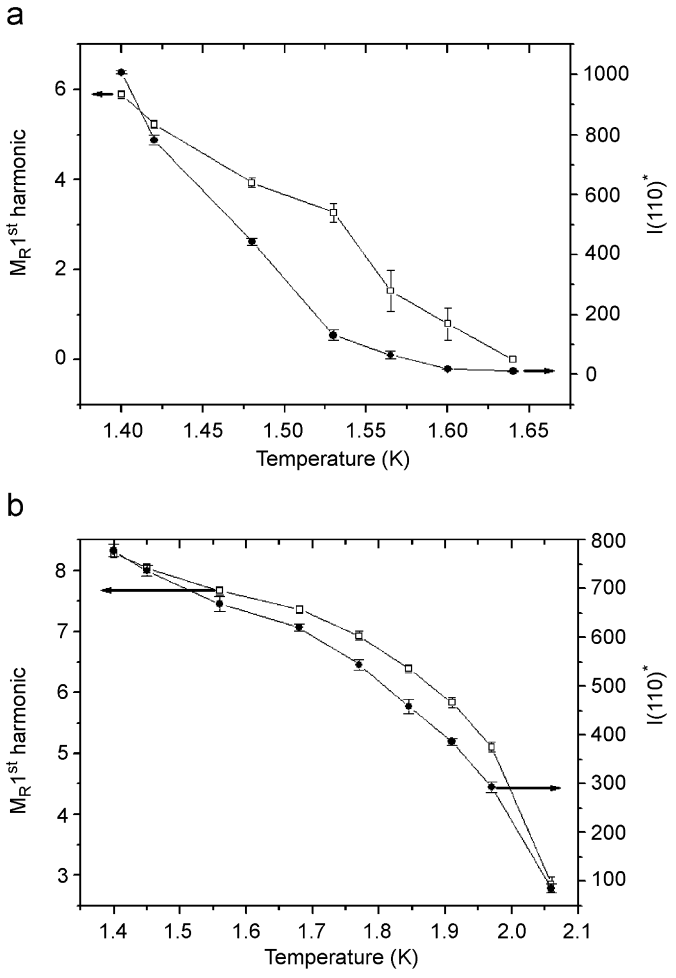

Fig. 12. Thermal variation of the integrated intensity of the 110^+ magnetic satellite ((●) right scale) and of the refined moment for the first harmonic ((■) left scale) for K_2TbF_6 (a) and Rb_2TbF_6 (b).

"The PCM, defined as the relative percentage of corners, edges and faces involved in the connection of the paramagnetic cations polyhedra, must be such as the percentage of edges is at least 50% for a long-range magnetic order could be observed at $T > 1{,}4\,K$" in fluoroterbates. This edge sharing seems to be the requested environment for the establishment of $4f$–$4f$ superexchange interactions in fluoroterbated, such magnetic interactions, always weak being not commonly encountered in rare-earth magnetism.

So, this relationship between the anionic sublattice and the magnetic behavior of fluoroterbates is another argument for the existence of superexchange interactions couplings in such compounds, since dipolar interactions are independent of the anionic array.

Besides these considerations, the ferromagnetic exchange interactions in the chains are in competition with frustrated antiferromagnetic dipolar interactions between the chains. At 1.43 K the intrachain exchange interactions could be balanced by the interchain dipolar interactions. As a result, the strengthening of the frustrated interchain interactions may induce an increase of the period of the magnetic structure.

Thus the magnetic behavior of Li_2TbF_6 brings out an experimental argument for the existence of weak, but significant, superexchange interactions. Apart from the existence of superexchange interactions, one may wonder how the magnetic structure of Li_2TbF_6, built of two "domains" of about 30 cells with "down" spins chains and 30 cells with "up" spins chains, may be described:

- on the basis of the magnetic behavior of Tb^{4+} magnetic moments,
- on the basis of domains occurring in an antiferromagnetic frustrated material.

Considering the behavior of the Tb^{4+} magnetic moments, this magnetic structure and more especially its thermal evolution, illustrates a progressive ordering, first with magnetic correlation of one-dimensional character, followed by the establishment of a quasi-two-dimensional incommensurate magnetic structure. This two-dimensional character is related to the orientation of the propagation vector, perpendicularly to the chains. It implies that the modulation propagates from chain to chain, so that the $[TbF_6]^{2-}$ chains supporting the modulation form "magnetic slabs". The discontinuity observed at $T = 1.43\,K$ emphasizes the three-dimensional character of the frustrated magnetic structure, i.e., the strengthening of "inter-slabs" magnetic interactions. As these interactions take place in the pseudo-hexagonal cationic array, they can be associated with the magnetic frustration, their strengthening explaining the increase of the period of the magnetic structure, as mentioned above. Such behavior is quite analogous to that reported for the $CoNb_2O_6$ oxide, which is built of rutile chains arranged in a pseudo-hexagonal packing [19].

Considering the magnetic domains, this square-modulated magnetic structure may also be an intermediate state preceding a final ferromagnetic phase ($k = 0$), where the size of the "up" and "down" domains increases as the temperature decreases, until the propagation vector k vanishes. This mechanism would lead to a ferromagnetic structure unaffected by frustration.

4. Conclusion

The neutron diffraction study of the M_2TbF_6 (M = Li, K, Rb) fluorides confirmed the structural models previously established and allowed the determination of their magnetic structures. Incommensurate, square-modulated magnetic structures have been observed below $T_N = 2.02(1)$, 1.60(2) and 2.07(2) K for Li, K and Rb representatives, respectively. Rietveld refinements of the magnetic structures at the lowest temperatures led to $R_{mag} = 3.86\%$ $M_{Tb4+} = 6.41(1)\,\mu_B$, $R_{mag} = 2.43\%$ $M_{Tb4+} = 4.44(6)\,\mu_B$ and $R_{mag} = 2.17\%$ $M_{Tb4+} = 6.27(5)\,\mu_B$ for

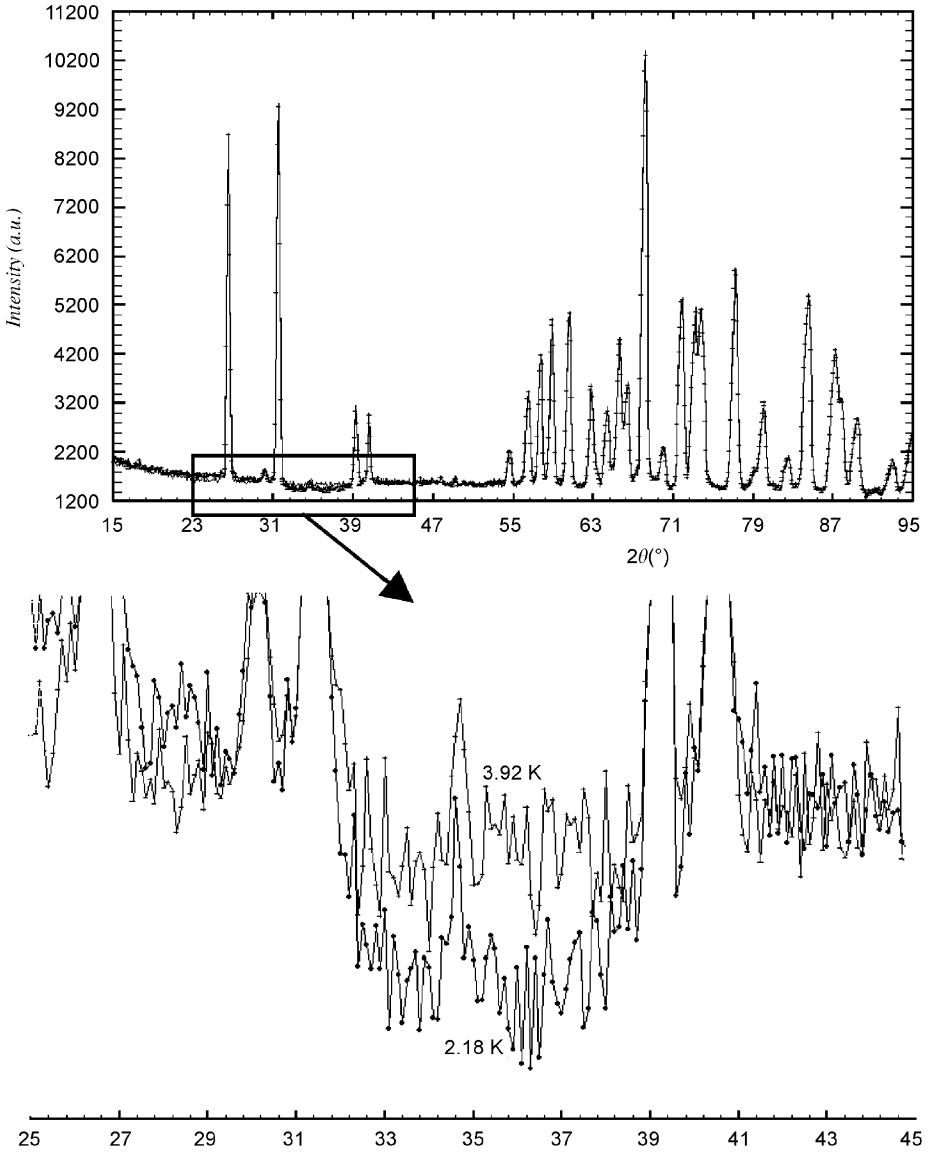

Fig. 13. Diffuse signal ascribable to one-dimensional magnetic correlations in Li_2TbF_6 ($\lambda = 2.4266$ Å).

Li_2TbF_6, K_2TbF_6 and Rb_2TbF_6, respectively, the theoretical moment of the Tb^{4+} free ion being 7.0 μ_B.

The magnetic behavior of the M_2TbF_6 (M = Li, K, Rb) fluorides has been rationalized by considering the $[TbF_6]^{2-}$ chains as the magnetic object from which the magnetic structure is constituted. The ordering temperatures observed in the M_2TbF_6 fluorides have been correlated to the efficiency of the dipolar interactions coupling the chains to relay the frustration induced by their pseudo-hexagonal packings.

The particular thermal evolution of the magnetic properties of Li_2TbF_6, with a greater period of the incommensurate magnetic structure at $T = 1.43$ K, has been related to the nature of magnetic interactions involved in the intra- and interchains magnetic couplings. The magnetic behavior of Li_2TbF_6 suggests the existence of superexchange interactions in the chains, while dipolar interactions likely occur between the chains. The superexchange, involving the fluoride ions, may be related to Goodenough–Kanamori–Anderson type magnetic interactions [20]. Such a mechanism, involving the participation of the 5*d* orbitals, has been suggested by L. Roy and T. Hughbanks in the Gd_2Cl_3 compound [21].

Further developments concerning the magnetic properties of tetravalent terbium fluorides proceed by the detailed study of fluoroterbates of various dimensionalities such as the dimorphic $BaTbF_6$ compound (1D and 3D for α and β polymorphs, respectively) or the two-dimensional $MTbF_5$ (M = K, Rb, Cs) fluorides.

References

[1] Y. Laligant, A. Le Bail, G. Ferey, D. Avignant, J.C. Cousseins, Eur. J. Solid State Inorg. Chem. 25 (1988) 551.

[2] M. Guillot, M. El-Ghozzi, D. Avignant, G. Ferey, J. Solid State Chem. 97 (2) (1992) 400.
[3] M. El-Ghozzi, D. Avignant, J. Fluor. Chem. 107 (2001) 229.
[4] M. Guillot; M. El-Ghozzi, D. Avignant, G. Ferey, C.R. Acad. Sci., Ser. II 313 (10) (1991) 1141.
[5] M. Josse, M. Dubois, M. El-Ghozzi, D. Avignant, G. André, F. Bourée, M. Guillot, J. Alloys Compd. 374 (2004) 207.
[6] T. Roisnel, J. Rodriguez-Carvajal, M. Pinot, G. Andre, F. Bouree, Mater. Sci. Forum 245 (1994) 166.
[7] J. Rodriguez-Carvajal, Abstracts of the Satellite Meeting on Powder Diffraction of the XV Congress of the IUCr, Toulouse, France, 1991, p. 127.
[8] E. Largeau, M. El-Ghozzi, D. Avignant, M. Guillot, F. Bourée, G. André, A. Cousson, J. Magn. Magn. Mater. 261 (2003) 93.
[9] M. El-Ghozzi, University Thesis, Clermont-Ferrand, 1992.
[10] V. Gaumet, University Thesis, Clermont-Ferrand, 1996.
[11] R. Hoppe, B. Melhorn, Zeit. Anorg. Allg. Chem. 425 (1976) 200.
[12] G. Demazeau, F. Menil, J. Portier, P. Hagenmuller, C.R. Acad. Sci. Paris 273 (1971) 1641.
[13] M.A. Pimenta, P. Licinio, Phys. Rev. B 50 (2) (1994) 722.
[14] A. Herpin, in: PUF (Ed.), Théorie du magnétisme, 1968, p. 587.
[15] T. Oguchi, Phys. Rev. 133 (1964) A1098.
[16] M. Josse, University Thesis, Clermont-Ferrand, 2003.
[17] N. El Khayati, R. Cherkaoui El Moursli, J. Rodriguez-Carvajal, G. André, N. Blanchard, F. Bourée, G. Collin, T. Roisnel, Eur. Phys. J. B 22 (2001) 429.
[18] M. Josse, M. El-Ghozzi, M. Dubois, D. Avignant, G. André, F. Bourée, Physica B 350 (1–3, Suppl. 1) (2004) E43.
[19] S. Kobayashi, S. Mitsuda, K. Hosoya, H. Yoshizawa, T. Hanawa, M. Ishikawa, K. Miyatani, K. Saito, K. Kohn, Physica B 213–214 (1995) 176.
[20] J.B. Goodenough (Ed.), Magnetism and the Chemical Bond, Wiley, New York, 1963.
[21] L. Roy, T. Hughbanks, J. Solid State Chem. 176 (2003) 294–305.